nature neuroscience

An acetylcholine-activated microcircuit drives temporal dynamics of cortical activity

Naiyan Chen[1–3], Hiroki Sugihara[1,3] & Mriganka Sur[1]

Cholinergic modulation of cortex powerfully influences information processing and brain states, causing robust desynchronization of local field potentials and strong decorrelation of responses between neurons. We found that intracortical cholinergic inputs to mouse visual cortex specifically and differentially drive a defined cortical microcircuit: they facilitate somatostatin-expressing (SOM) inhibitory neurons that in turn inhibit parvalbumin-expressing inhibitory neurons and pyramidal neurons. Selective optogenetic inhibition of SOM responses blocked desynchronization and decorrelation, demonstrating that direct cholinergic activation of SOM neurons is necessary for this phenomenon. Optogenetic inhibition of vasoactive intestinal peptide-expressing neurons did not block desynchronization, despite these neurons being activated at high levels of cholinergic drive. Direct optogenetic SOM activation, independent of cholinergic modulation, was sufficient to induce desynchronization. Together, these findings demonstrate a mechanistic basis for temporal structure in cortical populations and the crucial role of neuromodulatory drive in specific inhibitory-excitatory circuits in actively shaping the dynamics of neuronal activity.

Cholinergic innervation of the neocortex by afferent axons originating in the nucleus basalis (NB) of the basal forebrain[1] is a fundamental mechanism for modulating cortical sensory processing by influencing brain states[2] and the temporal dynamics of neurons[3]. Specifically, acetylcholine (ACh) can induce a highly desynchronized state, as measured by the field potential activity of neuronal populations[2], accompanied by prominent firing rate–independent decorrelation between the spike activity of individual neurons[3]. Both desynchronization and decorrelation[4] are considered to enhance information processing via redundancy reduction[3] in alert, active and attentive conditions[5,6] through direct engagement of cholinergic mechanisms[5]. ACh acts via thalamocortical and intracortical pathways[7], which in turn may contribute to different neuromodulatory functions[3]. In particular, decorrelation has been shown to depend on local activation of intracortical pathways[3], whereas desynchronization has been linked to membrane potential fluctuations in cortical neurons[8] and to inhibition in cortical networks[9]. Earlier studies proposed a possible role for rhythmic-bursting layer 5 pyramidal neurons[2] in the generation of cortical synchronization by cholinergic inputs. However, recent computational and experimental studies have suggested that inhibitory neurons can drive decorrelation and sparse coding in the cortex[10–12] and experimental evidence indicates that inhibitory activity correlates with[13] and can induce[14] specific neuronal activity patterns.

The cellular and circuit mechanisms that underlie desynchronization and decorrelation observed during cortical cholinergic modulation remain unresolved, and several key questions remain open. Is ACh-induced desynchronization and decorrelation in the cortex driven by inhibitory neurons? If so, which subtypes of inhibitory neurons are responsible and how do their functional interactions with each other and other cell types in the cortical circuit contribute to brain state and neuronal spike correlation changes? Previous work has demonstrated cholinergic facilitation of non–fast-spiking (FS) inhibitory neurons[15–17] including SOM[17–19], vasoactive intestinal peptide–expressing (VIP)[17,20,21] and layer 1 (L1) inhibitory neurons[20,22,23]. However, when and under what conditions ACh drives these different neuron types, and the specific functional circuit and causal pathway by which ACh carries out desynchronization and decorrelation, remain unresolved. We found that SOM neurons were active at a greater dynamic ACh range than VIP and L1 neurons, and cholinergic inputs to the superficial layers of primary visual cortex (V1) acted via SOM neurons (but not VIP and L1 neurons) to activate a specific inhibitory-excitatory cortical circuit that drives alterations of brain state synchrony and neuronal correlations.

RESULTS

Cortical dynamics evoked by optogenetic ACh release

We stimulated ACh release in superficial V1 *in vivo* of urethane-anesthetized adult mice (Online Methods) by cortical photostimulation of channelrhodopsin2 (ChR2)-expressing cholinergic axons from the basal forebrain in ChAT-ChR2 transgenic mice (**Fig. 1a**). This induced robust desynchronization of the local field potential (LFP) in V1 (ref. 24), similar to that induced by electrical stimulation of the nucleus basalis[25] (**Fig. 1b,c** and **Supplementary Fig. 1a–e**), including a post-stimulation decrease of low-frequency events (<10 Hz) and an increase of high-frequency events (10–100 Hz) (**Fig. 1d**).

One of the ways ACh[3] and attention[6] have been proposed to enhance the representation of information is through decorrelation of neuronal responses, but the mechanisms underlying such decorrelation are unclear. We next examined whether activation of neocortical cholinergic axons can induce decorrelation by measuring the activity

[1]Picower Institute for Learning and Memory, Department of Brain and Cognitive Sciences, Massachusetts Institute of Technology, Cambridge, Massachusetts, USA. [2]Singapore Bioimaging Consortium, Biomedical Sciences Institutes, Agency for Science, Technology and Research, Helios, Singapore. [3]These authors contributed equally to this work. Correspondence should be addressed to M.S. (msur@mit.edu).

Received 7 January; accepted 13 March; published online 27 April 2015; doi:10.1038/nn.4002

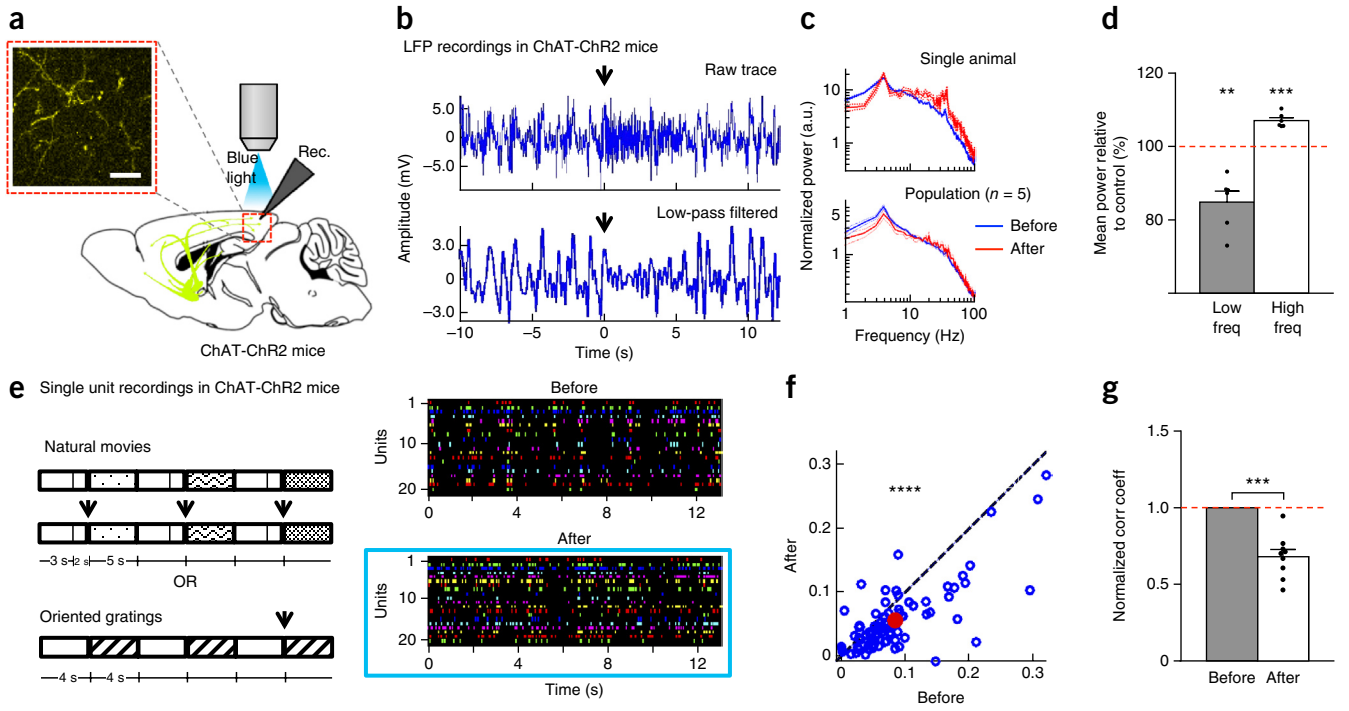

Figure 1 Optogenetic stimulation of ChAT-ChR2–expressing axons induces LFP desynchronization and decorrelation in layer 2/3 V1 neurons. (**a**) Experimental setup for LFP or single-unit recording, with ChAT-ChR2 blue light stimulation through the objective (adapted from *The Mouse Brain in Stereotaxic Coordinates*, Paxinos G. & Franklin K.B.J., Academic Press, 2001). Inset, fluorescence image of ChAT-ChR2 axons in V1. Scale bar represents 20 µm. (**b**) LFP desynchronization during ChAT-ChR2 stimulation at $t = 0$ s (arrows). Top, raw trace. Bottom, low-pass filtered < 5 Hz. (**c**) Top, example normalized power spectrum in an animal, 1 s before (blue) and after (red) ChAT-ChR2 stimulation, averaged over ten trials. Bottom, population mean normalized power spectrum across animals. Dotted lines indicate s.e.m. (**d**) ChAT-ChR2 stimulation induced a decrease in power of low-frequency events (<10 Hz, mean power relative to control ± s.e.m., 84.8 ± 2.99%, $P = 0.0039$, paired t test, $n = 5$ animals) and increase in high frequency events (10–100 Hz, 107 ± 0.776%, $P = 0.0003$, paired t test). (**e**) Left, visual and ChAT-ChR2 stimulation protocol. 'Natural movies' comprised three movies of 5-s duration (patterned boxes). 'Oriented gratings' comprised three trials of alternating 4 s of blank screen and 4 s of oriented gratings. ChAT-ChR2 stimulation is indicated by arrows. Right, an example experiment showing neuronal decorrelation before (control, top) and after ChAT-ChR2 stimulation (blue box, bottom). Each panel shows responses of multiple single units recorded simultaneously during presentation of natural movies. Each unit is indicated by a different color. (**f**) Scatter plot showing single-unit correlation coefficients before and after ChAT-ChR2 stimulation. Blue circles represent mean Pearson correlation coefficients for each neuron; red circle represents population-averaged correlation coefficient. $n = 85$ units from 9 animals, $P < 0.0001$, paired t test, comparing mean correlation coefficients for each unit before and after photostimulation. (**g**) ChAT-ChR2 stimulation induced a significant decrease in the population-averaged normalized correlation coefficient across experiments. $n = 9$ animals, $P = 0.0001$, paired t test, comparing population averaged correlation coefficients across animals before and after photostimulation. Error bars in **d** and **g** represent s.e.m. $^{**}P < 0.01$, $^{***}P < 0.001$, $^{****}P < 0.0001$.

of single units with an array of multiple electrodes (**Fig. 1a** and Online Methods) in response to both natural movies and gratings of random orientation (**Fig. 1e**). We observed substantial decorrelation between cortical neurons following photostimulation (**Fig. 1e**) at the level of single units (**Fig. 1f** and **Supplementary Fig. 1f**,**g**), as well as at the level of single pairwise correlations (**Supplementary Fig. 1h**) and experimental animals (**Fig. 1g** and **Supplementary Fig. 1i**).

Concentration-specific responses in non-FS interneurons

To test the hypothesis that inhibitory neurons can drive ACh-induced desynchronization and decorrelation, we first examined the cholinergic responses of several candidate non-FS inhibitory neurons known to be active during cholinergic modulation[15,16]. We performed *ex vivo* whole-cell current-clamp recordings from SOM neurons (tdTomato-positive neurons in SOM-TD mice), VIP neurons (in VIP-TD mice) and L1 inhibitory neurons (in wild-type (WT) mice) (**Fig. 2a**). Indeed, ACh application evoked facilitatory responses in SOM[17–19] (but see ref. 20), VIP[17,20,21] and L1 neurons[20,22,23] (**Fig. 2b**,**c**). Notably, SOM neurons fired robustly to a wide range of ACh concentrations (1 µM to 10 mM), consistent with their low-threshold spiking properties (**Supplementary Fig. 2**)[18], whereas VIP and L1 neurons depolarized at 100 µM Ach, but fired only at 10 mM ACh (**Fig. 2b**,**c**).

It is well established that specific subsets of inhibitory neurons connect to each other[26,27]. We therefore hypothesized that ACh can also indirectly induce inhibitory synaptic currents (IPSCs) in SOM, VIP and L1 neurons through cholinergic activation of defined inhibitory connections between these neurons. Indeed, ACh application evoked a barrage of inward currents in SOM, VIP and L1 neurons recorded in voltage-clamp mode with high chloride internal solution in the presence of NBQX, an AMPA receptor antagonist (**Fig. 2d**,**e**). These responses were also concentration specific: ACh at 1–100 µM induced responses in VIP and L1 neurons, but only minimal responses in SOM neurons, whereas ACh at 10 mM induced large responses in all three cell types (**Fig. 2d**,**e** and **Supplementary Fig. 3d**). These inward currents largely consisted of summated IPSCs[15], as they were reduced in the presence of GABA antagonists, particularly at lower ACh concentrations (1–100 µM; **Supplementary Fig. 3a**–**d**). Collectively, these findings suggest that the level of activation of SOM, VIP and L1 neurons, and the inhibitory inputs received by them, can change dynamically with different levels of cholinergic drive.

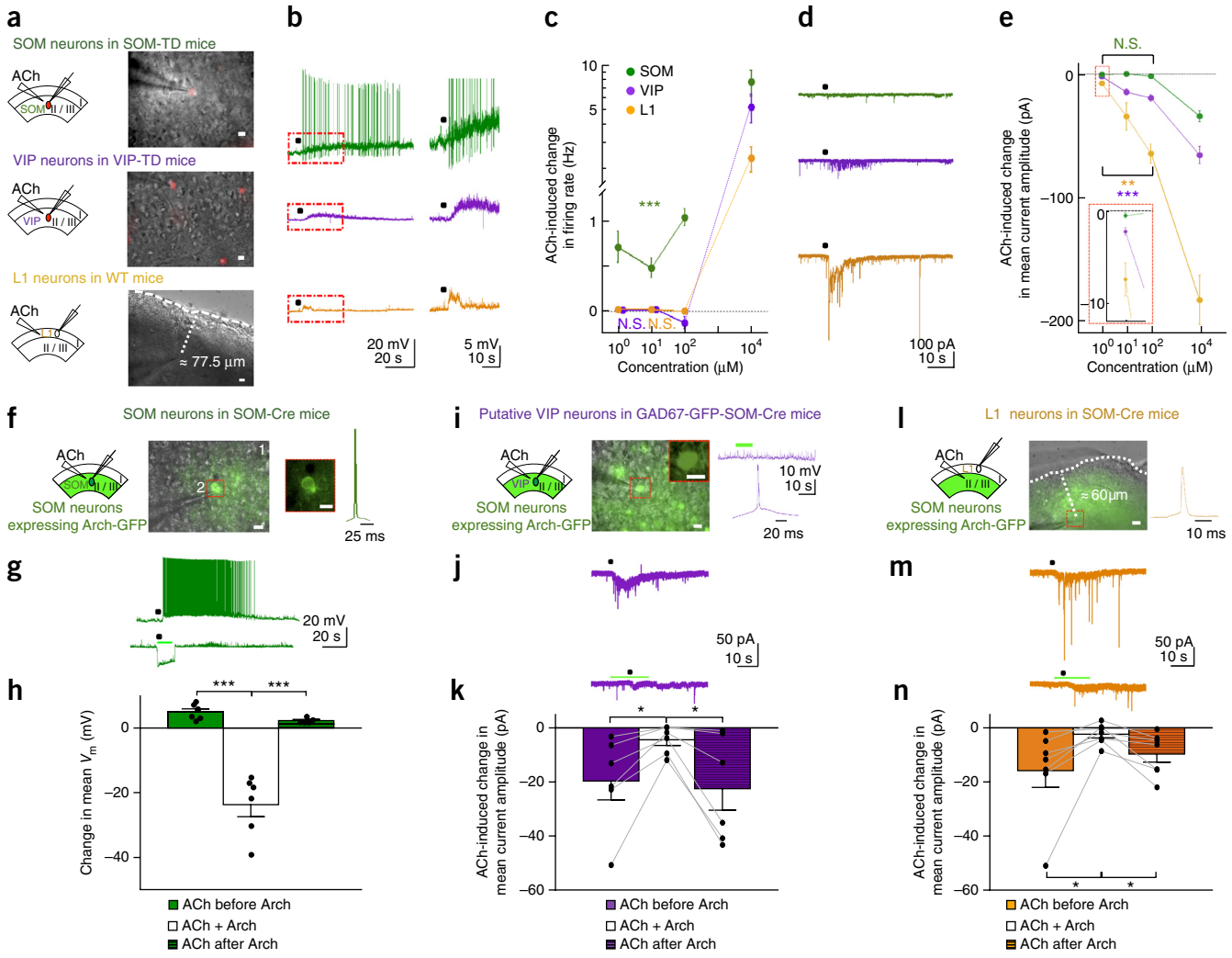

Figure 2 ACh induces facilitation at different dynamic ranges in layer 2/3 SOM, VIP and L1 inhibitory neurons in V1 slices. VIP and L1 neurons also receive inhibitory input from SOM neurons. (**a**) Merged fluorescence and differential interference contrast (DIC) images of a tdTomato-positive SOM neuron patched in a SOM-TD slice (top), VIP neuron in VIP-TD slice (middle) and L1 neuron in WT slice (bottom). Scale bars represent 10 µm. Inset, configuration of whole-cell patch-clamp recording in slices during ACh application. Experiments in **b**, **c**, **g** and **h** were performed with low-chloride internal solution in current-clamp mode. Experiments in **d**, **e**, **j**, **k**, **m** and **n** were recorded in voltage-clamp mode with high-chloride internal solution in NBQX. (**b**) Left, local ACh application (black dot, 100 µM) evoked a transient train of action potentials in SOM neurons (top) and depolarization in VIP (middle) and L1 neurons (bottom). Right, the same traces demarcated by dotted red lines on the left in expanded scales. (**c**) Population mean of ACh-induced changes in firing rate (Hz) of SOM, VIP and L1 neurons against ACh pipette concentrations. Error bars indicate 0.5 s.e.m. *y* axis is plotted in both linear (0–1.25) and log scale (>1.25). SOM, $n = 16$ neurons in 16 slices from 7 animals, $P = 0.00021$; VIP, $n = 8$ neurons in 7 slices from 4 animals, $P = 0.4736$; L1, $n = 7$ neurons in 7 slices from 3 animals, $P = 0.1639$; paired *t* test, comparing firing rate changes evoked by 1–100 µM ACh with null responses. (**d**) Local ACh application (black dot, 100 µM) evoked smaller NBQX-insensitive inward currents in SOM neurons (top) than in VIP (middle) and L1 neurons (bottom). (**e**) Data are presented as in **c**, but for ACh-induced changes in mean current amplitude (pA). Inset shows responses on an expanded scale. SOM, $n = 9$ neurons in 9 slices from 3 animals, $P = 0.0809$; VIP, $n = 10$ neurons in 10 slices from 4 animals, $P = 0.000172$; L1, $n = 8$ neurons in 7 slices from 3 animals, $P = 0.00726$; paired *t* test, comparing responses at 1–100 µM ACh with null responses. (**f**) Left, data are presented as in **a** for layer 2/3 of SOM-Cre slices in which AAV-flex-Arch-GFP virus was injected (shaded green). Middle, merged fluorescence and DIC images of a GFP-positive, Arch-expressing SOM neuron patched in a SOM-Cre slice. Relative positions of ACh pipette (1) and patch pipette (2) were as indicated. Inset, magnified image of the SOM neuron patched in previous image. Scale bars represent 10 µm. Right, a typical spike of a SOM neuron. (**g**) Local ACh application (black dot, 10 mM) evoked a transient train of action potentials in an Arch-expressing SOM neuron that was abolished by green light exposure (green bar). (**h**) Population average of mean V_m of SOM neurons when ACh was applied before, during and after Arch. $n = 6$ neurons in 6 slices from 3 animals, $P = 0.0003$, paired *t* test, comparing ACh-induced depolarization in SOM neurons before (4.96 ± 1.00 mV) and after Arch activation (–23.6 ± 3.80 mV). (**i**) Left and middle, data are presented as in **f**, where a layer 2/3 putative VIP neuron identified as expressing GFP, but not Arch, and being regular-spiking in a GAD67-GFP-SOM-Cre slice was recorded. Scale bar represents 10 µm. Note that the neuron is completely filled with GFP, in contrast with the annular membrane-bound Arch-GFP filling observed in **f**. Scale bar represents 10 µm. Top right, the VIP neuron was identified as not expressing SOM, as it did not hyperpolarize with green light exposure (green bar). Bottom right, a typical spike of a VIP neuron. (**j**) Local ACh application (black dot; 100 µM) evoked IPSCs in a putative VIP neuron that were reduced by green light exposure (green bar). (**k**) Population average of ACh-induced changes in mean current amplitude of putative VIP neurons before, during and after Arch. $n = 6$ neurons in 6 slices from 3 animals, $P = 0.0342$, paired *t* test, comparing ACh-induced current amplitudes before (–19.7 ± 7 pA) and after Arch (–4.40 ± 2.09 pA). (**l**) Data are presented as in **f**, where a L1 neuron in a SOM-Cre slice was recorded. Scale bar represents 10 µm. (**m**) Data are presented as in **j**, but for a L1 neuron. (**n**) Data are presented as in **k**, but with L1 neurons. $n = 7$ neurons in 7 slices from 4 animals, $P = 0.0389$, comparing ACh-induced current amplitudes before (–15.8 ± 6.20 pA) and after Arch (–2.34 ± 1.41 pA). Error bars in **h**, **k** and **n** represent s.e.m. $^*P < 0.05$, $^{**}P < 0.01$, $^{***}P < 0.001$, N.S., not significant. ACh was applied at 200 ms, 20 psi (**Supplementary Fig. 3**).

Recent work[26] indicates that SOM neurons avoid inhibiting one another, but provide substantial inhibition to all of the other inhibitory neurons, including VIP and L1 neurons. VIP neurons, on the other hand, provide inhibition nearly exclusively to SOM neurons, albeit at a level several-fold weaker than SOM-VIP and SOM-L1 inhibition (but see ref. 28). We hypothesized that the cholinergic drive–dependent responses observed in SOM, VIP and L1 neurons are a result of Ach-induced facilitation and indirect ACh activation of interneuron-specific inhibitory connections. In particular, the activation of SOM neurons could induce inhibition in VIP and L1 neurons to suppress the ACh-induced facilitatory responses at lower ACh concentrations (**Supplementary Fig. 4a**). To test this hypothesis, we transiently blocked the activity of SOM neurons by selectively expressing archaerhodopsin-3 (Arch) in them via viral injection of a flexed Arch construct into V1 of SOM-Cre mice; in addition, we crossed SOM-Cre mice with GAD67-GFP mice (GAD67-GFP-SOM-Cre mice) to identify inhibitory neurons in conjunction with Arch blockade of SOM neurons. We carried out current- and voltage-clamp recordings in slices with ACh application before and during green light stimulation of Arch in SOM neurons (**Fig. 2f–n**), from specific cell types that were also identified by their electrophysiological characteristics (**Supplementary Fig. 4b**). Stimulation of Arch in SOM neurons indeed abolished their cholinergic responses (**Fig. 2f–h**). Control recordings from SOM neurons in SOM-TD mice without Arch expression showed that green light stimulation alone did not induce any changes in ACh-evoked responses (**Supplementary Fig. 4c**).

To test the causal relationship between the ACh-induced facilitation of SOM responses and ACh-induced IPSCs in VIP and L1 neurons, we carried out voltage-clamp recordings from putative VIP neurons (identified by their non-FS properties, presence of GFP in GAD67-GFP-SOM-Cre mice and absence of hyperpolarization with green light stimulation; **Fig. 2i**) and from L1 neurons (GFP-negative, non-SOM neurons in layer 1 of SOM-Cre mice; **Fig. 2l**), whereas ACh was administered at 100 μM. Indeed, photostimulation of Arch in SOM neurons substantially reduced the ACh-induced IPSCs in both putative VIP neurons (**Fig. 2j**,**k** and **Supplementary Fig. 3e**) and L1 neurons (**Fig. 2m**,**n** and **Supplementary Fig. 3f**). Thus, these data support the hypothesis that defined inhibitory connections between molecularly distinct, non-FS inhibitory subtypes and their intrinsic firing properties can shape their responses at different levels of cholinergic drive (**Supplementary Fig. 4a**).

ACh directly facilitates SOM neurons

We next investigated the role of SOM neurons in the densely connected microcircuit of SOM, parvalbumin-expressing (PV) inhibitory neurons and pyramidal (PYR) neurons[26] during cholinergic modulation using both *ex vivo* current and voltage whole-cell patch-clamp recordings (**Supplementary Fig. 5a**). For SOM neurons (in SOM-TD mice; **Supplementary Fig. 5b**), ACh evoked robust depolarization that persisted in the presence of glutamatergic and GABAergic antagonists (**Fig. 3a**,**b**), indicating that it was a result of direct action of ACh. This response was prolonged and peaked within 10 s (**Supplementary Fig. 5c**). In addition, the response was reduced in the presence of the cholinergic antagonists mecamylamine and atropine (**Supplementary Fig. 6a**,**b**), indicating that both muscarinic and nicotinic receptors mediate this response.

In voltage-clamp recordings using low chloride internal solution, we observed a barrage of inward currents (**Supplementary Fig. 5d**) that comprised NBQX-insensitive muscarinic receptor– and nicotinic receptor–mediated currents (**Supplementary Fig. 6c–e**). We further confirmed that both muscarinic and nicotinic receptors are expressed in SOM neurons (**Supplementary Fig. 6f**). Thus, SOM neurons are directly activated via both types of receptors.

ACh-induced SOM-mediated IPSCs in PV neurons

Next, we characterized the cholinergic responses of PV neurons (in PV-TD mice; **Supplementary Fig. 5f**). ACh did not evoke any excitatory responses when recorded in current-clamp[15] (**Supplementary Fig. 5g**) and voltage-clamp modes with low chloride internal solution (**Supplementary Fig. 5h**), but induced IPSCs when recorded in voltage clamp mode with high chloride internal solution in the presence of NBQX (**Supplementary Figs. 5i** and **7a**). Thus, the ACh-induced responses in PV neurons require GABAergic transmission.

We hypothesized that the IPSCs in PV neurons were a result of activation of SOM neurons by ACh and subsequent inhibitory drive from SOM to PV neurons (**Fig. 3a**). To test this hypothesis, we carried out voltage-clamp recordings of IPSCs from putative PV neurons (identified by their FS properties and presence of GFP in GAD67-GFP-SOM-Cre mice) in slices containing Arch-expressing SOM neurons (**Fig. 3c** and **Supplementary Fig. 4b**). Indeed, photostimulation of Arch in SOM neurons reduced the ACh-induced increase in IPSCs in the putative PV neurons (**Fig. 3d**,**e** and **Supplementary Fig. 7c**), suggesting that ACh-induced facilitation of SOM responses can induce IPSCs in PV neurons.

ACh-induced SOM-mediated IPSCs in PYR neurons

Next, we investigated whether ACh-induced facilitation of SOM responses could induce IPSCs in PYR neurons. PYR neurons were identified as GFP-negative neurons in GAD67-GFP mice (**Supplementary Fig. 5j**) and recorded in voltage-clamp mode with high chloride internal solution in the presence of NBQX. ACh induced a barrage of IPSCs (**Supplementary Fig. 5m**) that also required GABAergic transmission (**Supplementary Fig. 7b**). To test whether cholinergic activation of SOM neurons contribute to the IPSCs in PYR neurons (**Fig. 3a**), we selectively recorded IPSCs from putative PYR neurons (identified by their pyramidal morphology and absence of GFP in SOM-Cre mice) in slices containing Arch-expressing SOM neurons (**Fig. 3f** and **Supplementary Fig. 4b**). Similar to PV neurons, photostimulation of Arch in SOM neurons reduced the ACh-induced increase in IPSCs in the putative PYR neurons (**Fig. 3g**,**h** and **Supplementary Fig. 7d**). Thus, these data reveal the circuit interactions between SOM, PV and PYR neurons in the context of ACh modulation: SOM neurons are directly activated by ACh and release GABA to evoke IPSCs in PV and PYR neurons (**Fig. 3a**).

Previous work has shown that cholinergic agonists can inhibit GABA release from PV neurons[29]. Because PV neurons widely inhibit PYR neurons[26,30], reduced GABA release from PV neurons can disinhibit PYR neurons[29] to facilitate excitatory synaptic events[31]. It is therefore possible that disinhibition of PYR neurons can occur via SOM-mediated PV inhibition. To investigate this mechanism, we recorded ACh-induced responses in low-chloride solution (**Supplementary Fig. 5l**). Indeed, ACh induced a barrage of inward currents that were reduced by NBQX (**Supplementary Fig. 8a–c**), consistent with this response comprising summated excitatory synaptic events[32]. These excitatory currents were also reduced by GABA antagonist (**Supplementary Fig. 8d–f**), supporting the presence of inhibitory neuron-mediated disinhibition. The prolonged component of this response, however, remained in the presence of

glutamatergic or GABAergic antagonists (**Supplementary Fig. 8b**,**e**), suggesting possible roles of intrinsic cholinergic mechanisms[33,34].

To further investigate the role of SOM neurons in mediating possible transient PYR neuronal disinhibition, we performed recordings of these inward currents in slices containing Arch-expressing SOM neurons. Indeed, photostimulation of Arch in SOM neurons also transiently blocked the ACh-induced excitatory currents in PYR neurons (**Supplementary Fig. 8g–i**). Similarly, the prolonged component was not abolished by SOM hyperpolarization (**Supplementary Fig. 8h**). These data collectively suggest the presence of a circuit comprising multiple pathways that can powerfully modulate PYR neuronal responses: direct inhibition by SOM neurons on PYR neurons, indirect disinhibition via PV on PYR neurons and an intrinsic response. These pathways may together induce the diverse subthreshold hyperpolarizing and depolarizing responses[32] revealed in current-clamp recordings of single PYR neurons (**Supplementary Fig. 5k**), leading to no change in firing at the population level *in vivo* (see below).

ACh evokes specific responses in SOM, PV and PYR neurons

Our findings highlight the role of cholinergic-activated SOM neurons acting as a powerful hub of inhibition to modulate principal neurons in the cortex, thereby making it a strong candidate to mediate ACh-induced temporal changes in neuronal activity. Before probing the possible causal link between the SOM-driven microcircuit and LFP desynchronization/neuronal decorrelation, we first examined whether cholinergic responses *in vivo* were consistent with those observed *ex vivo*. We performed *in vivo* targeted cell-attached recordings from identified red fluorescent protein (RFP)-labeled SOM neurons (labeled with viral injection of a *loxP*-flanked RFP construct in V1 of ChAT-ChR2 mice crossed with SOM-Cre mice) and PV neurons (similarly labeled in ChAT-ChR2-PV-Cre mice), as well as *in vivo* recording of putative PYR neuron single units (in ChAT-ChR2 mice) in the superficial layers of V1 (**Fig. 4**). Neuron types were also distinguished by their spike shape (**Supplementary Fig. 9**). Indeed, cholinergic responses induced by activation of ChAT-ChR2 axons *in vivo* were consistent with those observed

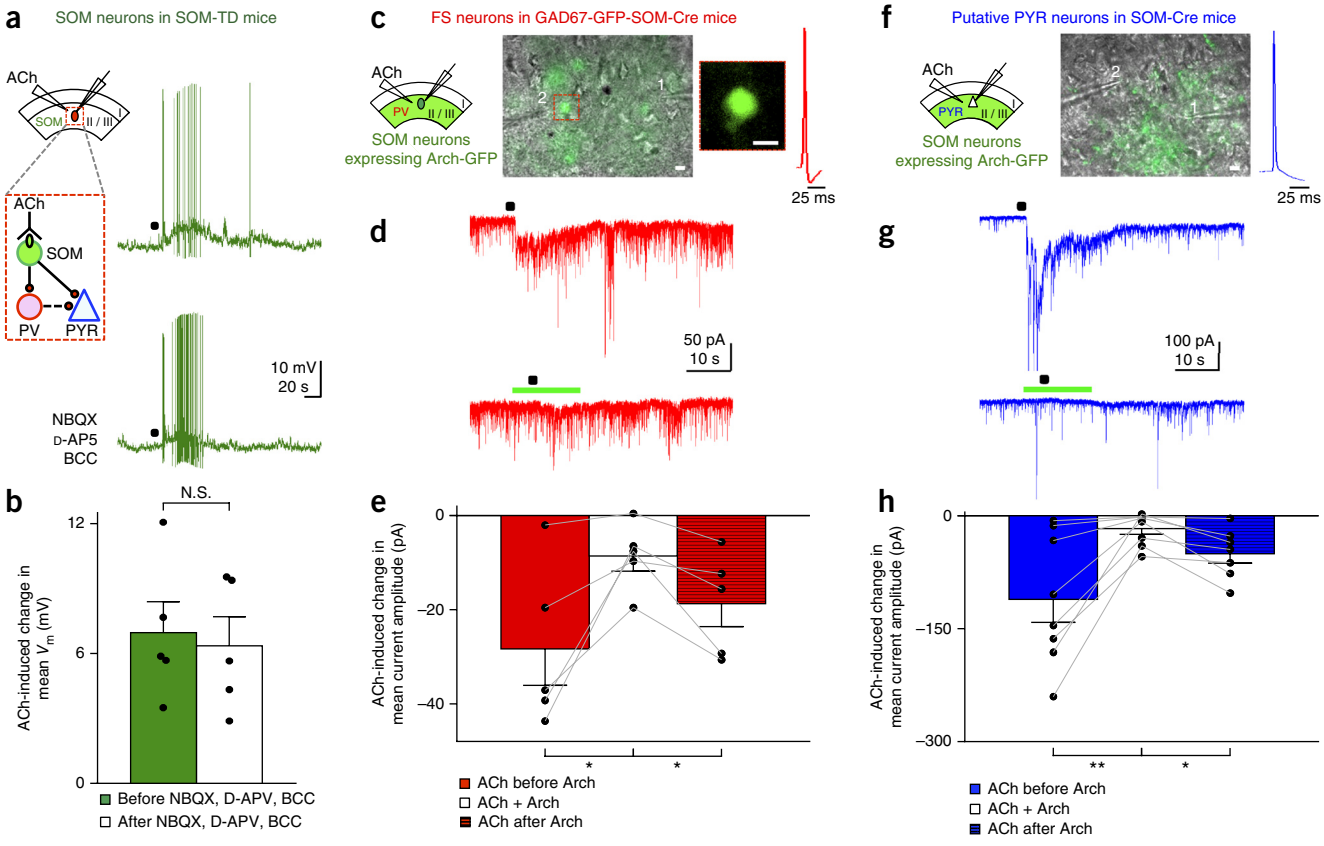

Figure 3 Direct cholinergic facilitation of SOM responses leads to indirect inhibitory responses in FS (putative PV) and PYR neurons. Recordings in **a** and **b** were recorded with low-chloride internal solution in current-clamp mode. Recordings in **d**, **e**, **g** and **h** were recorded in voltage-clamp mode with high-chloride internal solution in NBQX. (**a**) Local ACh application (black dot) evoked a transient train of action potentials in SOM neurons (in SOM-TD slices) that persisted in the presence of NBQX, D-AP5 and BCC. Inset, proposed mechanism of cholinergic action on SOM, PV and PYR neurons. Red circles and green ovals indicate inhibitory synapses and cholinergic receptors, respectively. (**b**) Population average of ACh-induced changes in mean V_m of SOM neurons before and after bath application of glutamatergic and GABAergic antagonists. $n = 5$ neurons in 5 slices from 3 animals, $P = 0.565$, comparing ACh-induced change in mean V_m before (6.96 ± 1.44 mV) and after NBQX, D-AP5 and BCC (6.35 ± 1.34 mV). (**c**) Data are presented as in **Figure 2i**, where GFP-positive, non–Arch-expressing, FS neurons in a GAD67-GFP-SOM-Cre slice were recorded. Scale bars represent 10 µm. (**d**) Local ACh (black dot) evoked IPSCs in a GFP-positive FS neuron that was reduced by green light (green bar). (**e**) Population average of ACh-induced changes in mean current amplitude of GFP-positive neurons before, during and after Arch. $n = 5$ neurons in 5 slices from 3 animals, $P = 0.0385$, paired t test, comparing ACh-induced current amplitudes before (–28.3 ± 7.74 pA) and after Arch (–8.59 ± 3.23 pA). (**f**) Data are presented as in **Figure 2f**, where a GFP-negative, putative PYR neuron in a SOM-Cre slice was recorded. Scale bar represents 10 µm. (**g**) Data are presented as in **d**, but in a putative PYR neuron. (**h**) Data are presented as in **e**, but with putative PYR neurons. $n = 8$ neurons in 8 slices from 4 animals, $P = 0.0091$, comparing ACh-induced current amplitudes before (–111.1 ± 30.6 pA) and after Arch (–17.1 ± 7.58 pA). Error bars in **b**, **e** and **h** represent s.e.m. $^*P < 0.05$, $^{**}P < 0.01$, N.S., not significant. ACh was applied at 10 mM, 200 ms, 20 psi (**Supplementary Fig. 7**).

ex vivo. Robust facilitatory responses were observed in SOM neurons (**Fig. 4b**,**c**), whereas suppressive responses were observed in PV neurons (**Fig. 4e**,**f**). In putative PYR neurons, however, there was no change in response rate (**Fig. 4h**,**i**). Thus, endogenous ACh release via photostimulation evokes distinct *in vivo* signatures from SOM, PV and PYR neurons: SOM neurons are facilitated, PV neurons are suppressed, and the mean spike rate of PYR neurons does not change, but their visual responses are decorrelated.

ACh-induced cortical dynamics is mediated by SOM neurons

We next examined whether SOM neurons can mediate the ACh-induced changes in temporal dynamics of cortical activity, including LFP desynchronization and neuronal decorrelation (**Fig. 1**). To establish a causal relationship between these phenomena and SOM neurons, we expressed Arch in SOM neurons by viral injection in ChAT-ChR2-SOM-Cre mice (**Fig. 5a**). Blue light–induced ChAT-ChR2 stimulation facilitated SOM neurons, but green light activation of Arch simultaneously with blue light stimulation of ACh release blocked the facilitation and even reduced responses below background, consistent with hyperpolarization of SOM neurons by Arch (**Fig. 5b**,**c**). The LFP in the Arch-injected V1 area was desynchronized after activation of ChAT-ChR2 axons; however, this modulation was absent when Arch was activated (and SOM neurons transiently inactivated) during ChAT-ChR2

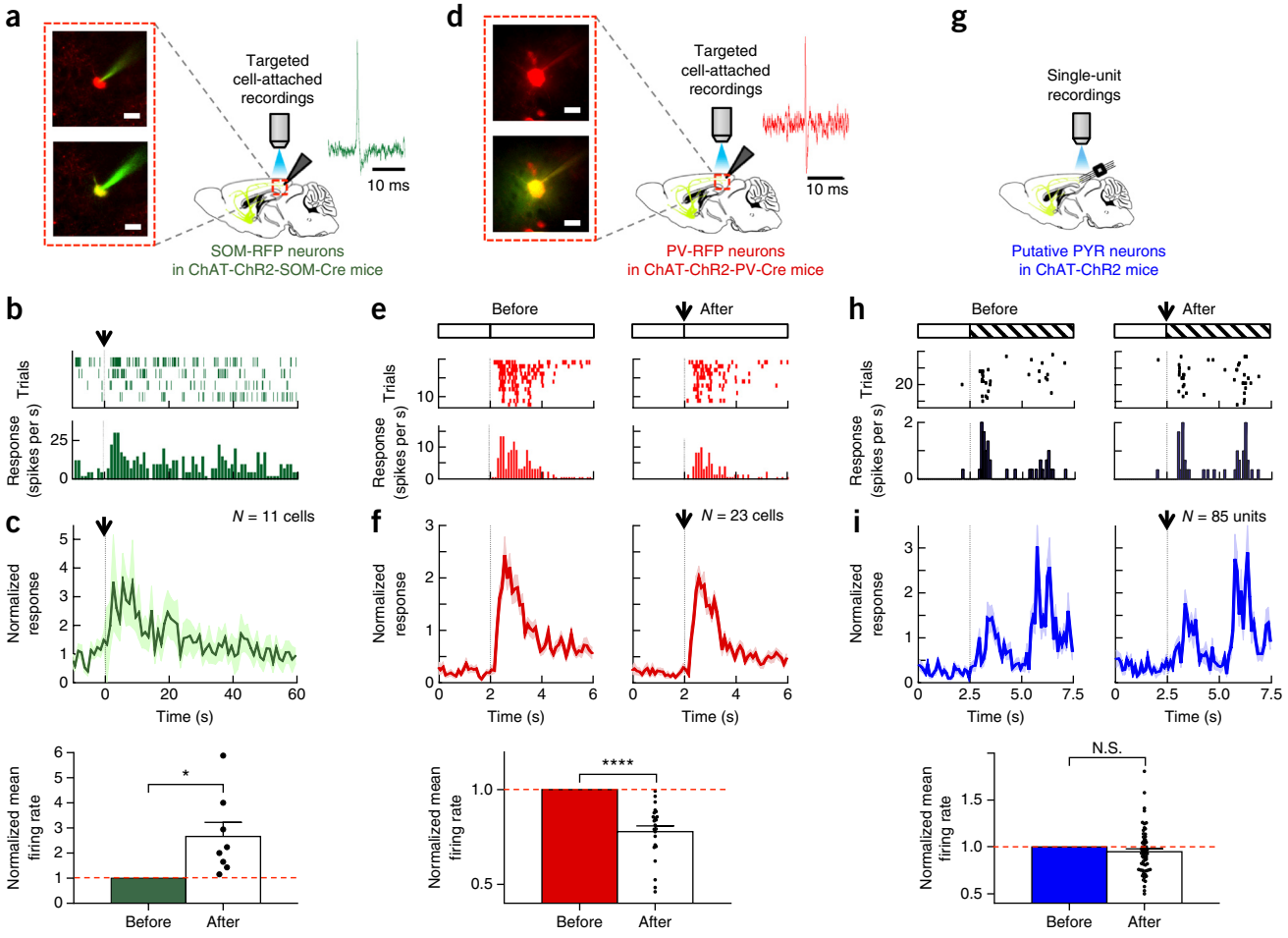

Figure 4 Optogenetic stimulation of ChAT-ChR2–expressing axons evokes diverse responses in V1 layer 2/3 SOM, PV and putative PYR neurons. (**a**) Experimental setup for two photon–guided, cell-attached recording of labeled SOM neurons during ChAT-ChR2 blue light stimulation through objective. Left inset, RFP-positive SOM cells (red) were targeted with a glass pipette containing Alexa 488 dye (green, top). Bottom, the cell was filled to confirm its identity after recording. Scale bars represent 20 µm. Right inset, a typical spike of a SOM neuron in a ChAT-ChR2-SOM-Cre animal. (**b**) Raster plot (top) and peri-stimulus time histogram (PSTH) (bottom) of responses of a SOM neuron to ChAT-ChR2 stimulation (arrow). (**c**) Top, normalized PSTH of the responses of SOM neurons to ChAT-ChR2 stimulation (arrow). Bottom, normalized mean firing rate 8 s before and after ChAT-ChR2 stimulation ($n = 11$ neurons from 6 animals, $P = 0.023$, paired t test, comparing normalized firing rate before and after photostimulation; duration of response = 30.9 ± 7.49 s; baseline firing rate of SOM neurons = 1.26 ± 0.531 Hz). (**d**) Data are presented as in **a**, where RFP-positive PV neurons in ChAT-ChR2-PV-Cre mice were recorded. Scale bars represent 20 µm. (**e**) Raster plot (top) and PSTH (bottom) of visual responses of a PV neuron before (left) and after (right) ChAT-ChR2 stimulation (arrow). ChAT-ChR2 stimulation was synchronized to the start of orientation grating stimuli (patterned bar). A blank gray screen (white bar) preceded visual stimulation. (**f**) Top, normalized PSTH of the visual responses of PV neurons before (left) and after (right) ChAT-ChR2 stimulation (arrow). Bottom, normalized mean visual response (over 4 s) before and after ChAT-ChR2 stimulation ($n = 23$ neurons from 4 animals, $P < 0.0001$, paired t test, comparing normalized visual responses before and after photostimulation; baseline firing rate of PV neurons = 1.90 ± 0.542 Hz). (**g**) Experimental setup for single-unit recording in ChAT-ChR2 animals using a tungsten electrode array during ChAT-ChR2 blue light stimulation through the objective. (**h**,**i**) Data are presented as in **e** and **f**, but for putative PYR neurons. Random orientation grating or natural movie stimuli were used ($n = 85$ units from 9 animals, $P = 0.273$, paired t test, comparing normalized visual response before and after photostimulation; baseline firing rate of PYR neurons = 0.0865 ± 0.0242 Hz). $^*P < 0.05$, $^{****}P < 0.0001$. N.S., not significant. Shaded regions and error bars in **c**, **f** and **i** indicate s.e.m.

stimulation (**Fig. 5d**,**e**). This finding was consistent across different pre-stimulation cortical states (**Supplementary Fig. 10**). Control experiments in ChAT-ChR2 animals without Arch expression demonstrated that green light presentation was not sufficient to abolish the desynchronization (**Supplementary Fig. 11a**–**c**). Thus, these findings directly demonstrate that SOM neurons are critical for cholinergic-induced desynchronization of network activity in the superficial layers of V1.

To examine the effect of SOM neurons on decorrelation of neuronal activity, we carried out single-unit recordings in ChAT-ChR2-SOM-Cre

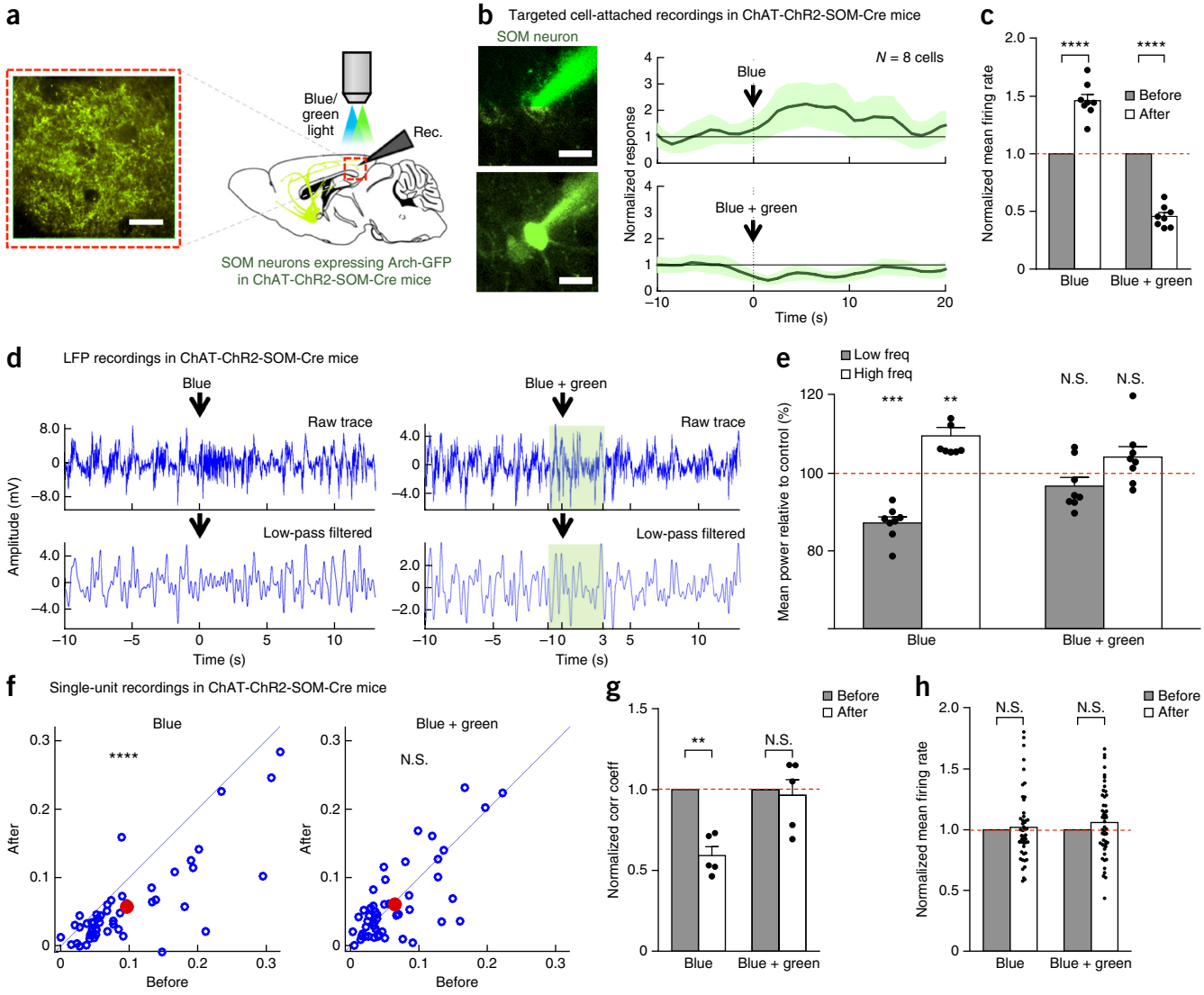

Figure 5 ChAT-ChR2 stimulation–induced LFP desynchronization and decorrelation is mediated by SOM neurons. (**a**) Experimental setup for electrophysiological recordings during ChAT-ChR2 blue light stimulation and SOM-Arch green light stimulation through the objective. Inset, image of Arch-GFP expression in V1. Scale bar represents 50 µm. (**b**) Top left, an Arch-expressing SOM neuron with membrane-bound GFP was targeted with a glass pipette containing Alexa 488 dye (green). Bottom, the cell was filled to confirm its identity after recording. Scale bars represent 10 µm. Right, normalized mean PSTH of responses of eight SOM neurons to ChAT-ChR2 stimulation (arrows, 1-s duration) without (top) and with (bottom) Arch stimulation (10-s duration, preceding ChAT-ChR2 stimulation by 1 s). Shaded area indicates s.e.m. (**c**) ChAT-ChR2 blue light stimulation induced an increase in the normalized mean firing rate measured 8 s before and after stimulation ($P < 0.0001$). SOM-Arch green light stimulation reversed this increase ($P < 0.0001$). $n = 8$ neurons from 4 animals, paired t test. (**d**) LFP desynchronization during ChAT-ChR2 stimulation at $t = 0$ s (arrows) (left) was blocked by Arch stimulation (green bar) (right). Top, raw trace. Bottom, low-pass filtered (<5 Hz). (**e**) ChAT-ChR2 blue light stimulation induced a decrease in power of low-frequency events (<10 Hz, 87.3 ± 1.50%, $P < 0.0001$) and increase in high-frequency events (10–100 Hz, 109.7 ± 2.12%, $P = 0.0026$) respectively. This was blocked during simultaneous SOM-Arch green light and ChAT-ChR2 blue light stimulation (low frequency, 96.7 ± 2.21%, $P = 0.180$; high frequency, 104.2 ± 2.63%, $P = 0.154$). $n = 8$ animals, comparison with null changes, paired t test. (**f**) Scatter plot showing the between-cell correlation coefficients before and after ChAT-ChR2 stimulation ($P < 0.0001$, paired t-test, left) and before and after simultaneous SOM-Arch and ChAT-ChR2 stimulation ($P = 0.432$, right). Each blue circle represents the average correlation coefficient between a single neuron and all other neurons in the same recording; the red circle is the population average. $n = 49$ units from 5 animals. (**g**) The population-averaged normalized correlation coefficient across experiments during ChAT-ChR2 blue light stimulation ($P = 0.0017$) and during simultaneous SOM-Arch green light and ChAT-ChR2 blue light stimulation ($P = 0.742$). $n = 5$ animals, paired t test. (**h**) Normalized mean visual response (over 4 s) during ChAT-ChR2 blue light stimulation ($P = 0.630$) and during simultaneous ChAT-ChR2 blue light and SOM-Arch green light stimulation ($P = 0.149$). $n = 49$ units from 5 animals, paired t test. Error bars in **c**, **e**, **g** and **h** represent s.e.m. $^{**}P < 0.01$, $^{***}P < 0.001$, $^{****}P < 0.0001$. N.S., not significant.

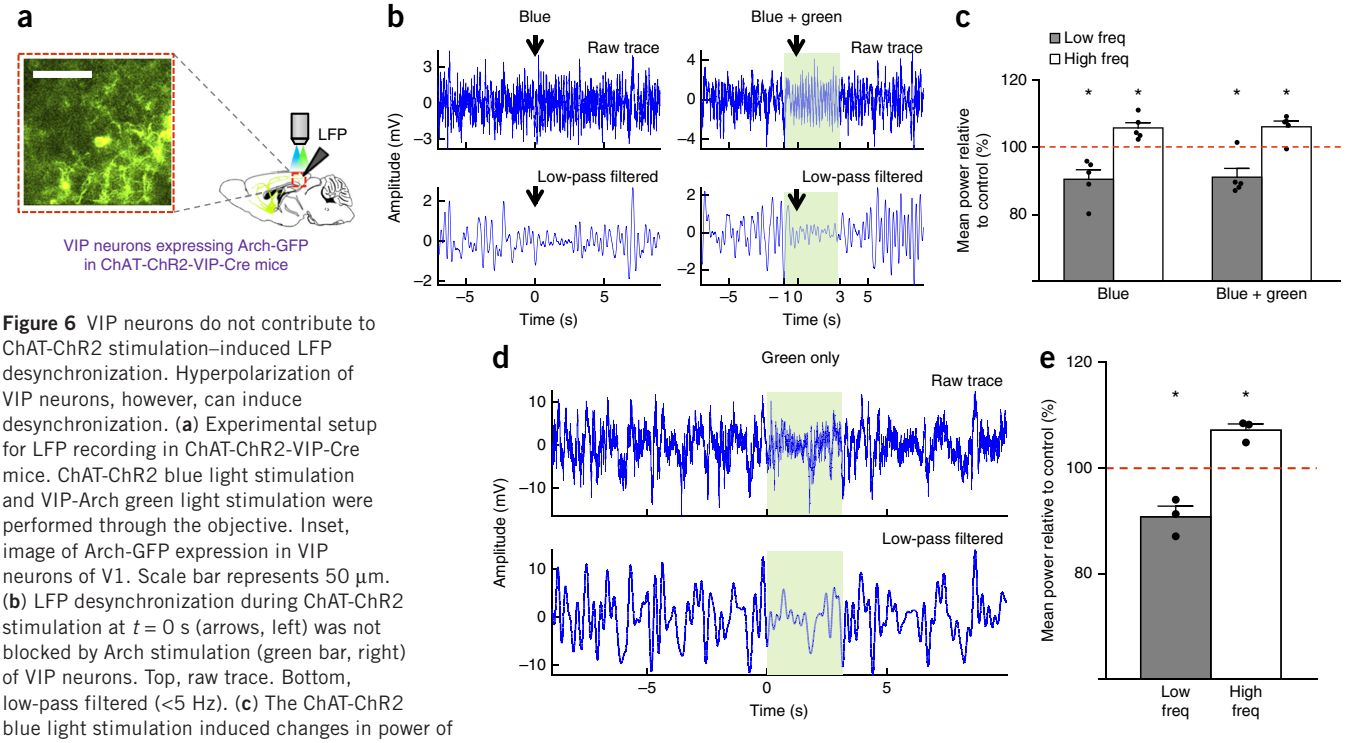

Figure 6 VIP neurons do not contribute to ChAT-ChR2 stimulation–induced LFP desynchronization. Hyperpolarization of VIP neurons, however, can induce desynchronization. (**a**) Experimental setup for LFP recording in ChAT-ChR2-VIP-Cre mice. ChAT-ChR2 blue light stimulation and VIP-Arch green light stimulation were performed through the objective. Inset, image of Arch-GFP expression in VIP neurons of V1. Scale bar represents 50 µm. (**b**) LFP desynchronization during ChAT-ChR2 stimulation at $t = 0$ s (arrows, left) was not blocked by Arch stimulation (green bar, right) of VIP neurons. Top, raw trace. Bottom, low-pass filtered (<5 Hz). (**c**) The ChAT-ChR2 blue light stimulation induced changes in power of low-frequency (<10 Hz, 90.5 ± 2.83%, $P = 0.0285$) and high-frequency events (10–100 Hz, 105.8 ± 1.58%, $P = 0.0209$) were not blocked during simultaneous VIP-Arch green light and ChAT-ChR2 blue light stimulation (low frequency, 91.1 ± 2.64%, $P = 0.0281$; high frequency, 106.2 ± 1.70%, $P = 0.0221$). $n = 5$ animals, paired t test. (**d**) LFP desynchronization during optogenetic Arch stimulation of VIP neurons (green bar). Top, raw trace. Bottom, low-pass filtered (<5 Hz). (**e**) Green light stimulation of Arch-expressing VIP neurons induced a significant decrease in power of low-frequency events (<10 Hz, 90.8 ± 2.02%, $P = 0.0448$) and increase in high-frequency events (10–100 Hz, 107.2 ± 1.17%, $P = 0.0254$) in ChAT-ChR2-VIP-Cre mice. $n = 3$ animals, paired t test. Error bars in **c** and **e** represent s.e.m. $^*P < 0.05$.

mice in the region of V1 in which Arch was expressed in SOM neurons (**Supplementary Fig. 12a**). ChAT-ChR2 activation with blue light induced decorrelation between neurons, but the decorrelation was blocked during green light activation of Arch (**Fig. 5f,g** and **Supplementary Fig. 12b**). In control ChAT-ChR2 experiments without Arch expression, green light alone did not alter the extent of decorrelation (**Supplementary Fig. 11d–f**). It is also worth mentioning that the decorrelation and its blockade by SOM hyperpolarization was observed to be firing rate independent (**Figs. 4i** and **5h** and **Supplementary Fig. 12c**), thereby implicating distinct mechanisms from spike rate–dependent correlation changes[35].

Decorrelation can improve visual coding by reducing redundancy between neurons[3]. We carried out a simple discrimination analysis[3] and found that decorrelation indeed improved discrimination performance; this improvement was also blocked by activation of Arch in SOM neurons (**Supplementary Fig. 12d**). Collectively, these data indicate that cholinergic activation of SOM neurons drives neuronal decorrelation in the superficial layers of V1 and thereby potentially contributes to enhanced information processing.

VIP and L1 neurons do not mediate ACh-induced IPSCs

Recent work has revealed direct, weak inhibition by VIP on SOM neurons[26] and indirect modulation of layer 5 PYR neurons by L1 neurons via layer 2/3 inhibitory neurons[27]. We examined whether these functional connections could modulate layer 2/3 PYR neurons to alter desynchronization/decorrelation during cholinergic modulation. We carried out voltage-clamp recordings from PYR neurons in VIP-Cre and 5HT3a-Cre slices containing Arch-expressing VIP neurons and Arch-expressing 5HT3a-Cre–positive L1 neurons (**Supplementary Fig. 13a,e**), respectively. Although the 5HT3aR-expressing interneurons are known to be heterogeneous[36], we targeted the optogenetic stimulation specifically to layer 1 of visual cortex. Notably, hyperpolarization of VIP neurons by Arch (**Supplementary Fig. 13a,b**) did not block, but instead facilitated, IPSCs in PYR neurons (**Supplementary Fig. 13c,d**). On the other hand, hyperpolarization of 5HT3aR-expressing L1 neurons by Arch (**Supplementary Fig. 13e,f**) had no effect on IPSCs in PYR neurons (**Supplementary Fig. 13g,h**). These findings suggest that VIP, but not L1, neurons can alter inhibitory transmission to layer 2/3 PYR neurons during cholinergic modulation, possibly through the VIP-SOM[26] connection (**Supplementary Fig. 4a**).

VIP neurons do not mediate ACh-induced cortical dynamics

We then examined the effect of VIP neurons on cortical desynchronization in ChAT-ChR2-VIP-Cre mice in which we expressed Arch specifically in VIP neurons. Hyperpolarization of VIP neurons did not have any effect on ChAT-ChR2–induced cortical desynchronization (**Fig. 6a–c**). This was also observed at a high power of ChAT-ChR2 stimulation (**Supplementary Fig. 10**). The conclusion held for a range of pre-stimulation cortical states observed in our recordings (**Supplementary Figs. 1a–d** and **10**). Thus, under our conditions, LFP desynchronization resulting from intracortical ACh release directly involves SOM neurons, but not VIP neurons.

In the absence of cholinergic stimulation, hyperpolarizing VIP neurons can induce IPSCs in PYR neurons (**Supplementary Fig. 13i,j**). To investigate whether hyperpolarizing VIP neurons can change cortical synchronization independent of the cholinergic pathway, we performed green light stimulation of ChAT-VIP-Arch animals. Indeed, VIP neuronal hyperpolarization in the absence

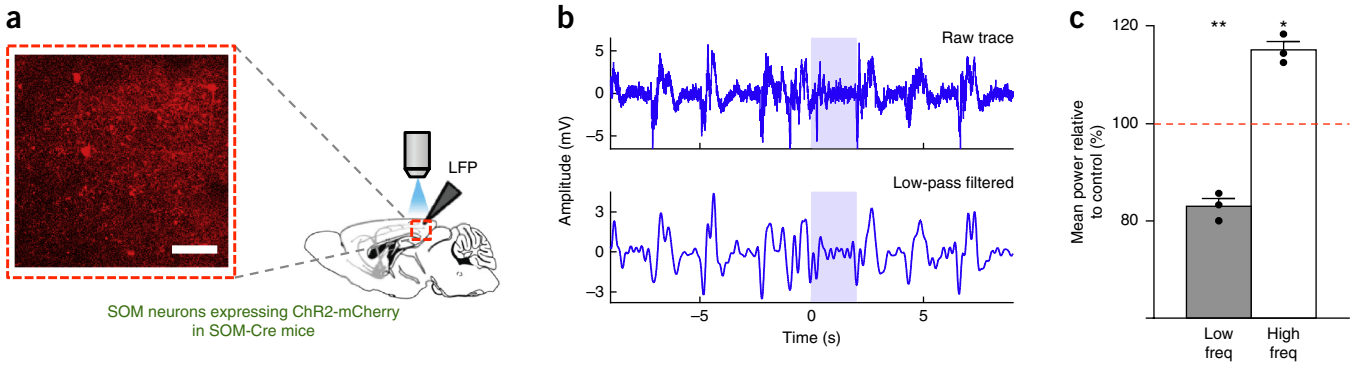

Figure 7 Direct ChR2 stimulation of SOM neurons is sufficient to induce LFP desynchronization. (**a**) Experimental setup for LFP recording in SOM-Cre mice during SOM-ChR2 blue light stimulation through the objective. Inset, image of ChR2-mCherry expression in SOM neurons of V1. Scale bar represents 50 µm. (**b**) LFP desynchronization during SOM-ChR2 stimulation (blue bar). Top, raw trace. Bottom, low-pass filtered (<5 Hz). (**c**) SOM-ChR2 stimulation induced a decrease in power of low-frequency events (81.7 ± 1.80%, $P = 0.0095$) and an increase in high-frequency events (116.8 ± 1.85%, $P = 0.0120$). $n = 3$ animals, paired t test. Error bars in **c** represent s.e.m. $^*P < 0.05$, $^{**}P < 0.01$.

of ChAT-ChR2 stimulation was also sufficient to induce cortical desynchronization (**Fig. 6d**,**e**). This can likely be explained by the inactivation of VIP-to-SOM inhibition (**Supplementary Fig. 4a**) and consequential activation of the microcircuit comprising SOM-PYR and SOM-PV-PYR connections to induce cortical desynchronization similar to that observed with ChAT-ChR2 stimulation.

SOM-activation is sufficient to evoke cortical dynamics

Our data reveal the important role of SOM neurons in driving ACh-induced desynchronization. A final question remains. Is direct SOM activation independent of the cholinergic pathway sufficient to evoke desynchronization? To enable direct activation of SOM neurons, we selectively expressed ChR2 in SOM neurons by viral injection in SOM-Cre mice (**Fig. 7a**). Indeed, blue light stimulation of ChR2-expressing SOM neurons induced robust desynchronization of LFP in V1 (**Fig. 7b**,**c**), similar to that observed during cholinergic modulation. Thus, these data suggests that direct SOM activation is sufficient to induce desynchronization and further establish the crucial role of SOM neurons in driving the temporal dynamics of cortical activity.

DISCUSSION

Decorrelation between neurons can enhance[3] and even optimize[7] information processing. During execution of attentional tasks, decorrelation has been demonstrated to enhance population sensitivity to stimulus changes and the signal-to-noise ratio of neural signals[6]. Our study provides, to the best of our knowledge, the first demonstration of a specific subtype of inhibitory neuron that can contribute to such temporal alterations of spike trains in the context of cholinergic modulation, a major neuromodulatory pathway that has been implicated in attention and arousal[5]. Specifically, we found that direct facilitation of SOM neurons at wide ranges of cholinergic drive can activate both direct inhibition and possibly indirect PV disinhibition on PYR neurons. The activation of this microcircuit can consequently drive a firing rate–independent decorrelation of PYR neuronal spike trains.

We further demonstrate that VIP and L1 neurons can also be facilitated by ACh, albeit effectively only at higher ACh concentration ranges due to inhibition by SOM neurons[26]. This finding is supported by previous work that has demonstrated stronger SOM-VIP and SOM-L1 than VIP-SOM connections[26] and is perhaps facilitated by the uniquely low threshold firing properties of SOM neurons (**Supplementary Fig. 2**)[18]. Although our findings (**Fig. 2c** and **Supplementary Fig. 1e**) support previous observations that cholinergic modulation of VIP neurons and cortical desynchronization is correlated with cholinergic drive[20], we did not observe any reduction of cholinergic-driven cortical desynchronization when VIP neurons were hyperpolarized. Instead, VIP hyperpolarization alone was able to induce cortical desynchronization, possibly through the disinhibition of SOM neurons[26] and the consequent activation of the SOM-driven microcircuit (**Fig. 6**). Collectively, our data clearly demonstrate that the cholinergic-activated inhibitory neuron subtypes[15,16,18,20–23] were not all active simultaneously, but were instead activated at different dynamic ranges, a finding that resolves some of the complexities of ACh mechanisms. Specifically, it is not clear whether all ACh-modulated cell types are involved simultaneously in all ACh-mediated brain functions. On the basis of these findings, we propose instead that cholinergic-activated cell types can reorganize themselves into specialized microcircuits that are engaged at different levels of cholinergic drive to mediate distinct brain functions. SOM neurons could have a crucial functional role in the active shaping of temporal structure of neural activity, whereas VIP and L1 neurons may contribute to functions requiring higher cholinergic drive such as gain control during locomotion[21] or associative fear learning[23].

Our results indicate that direct SOM activation via both muscarinic and nicotinic receptors by intracortical ACh is critical for the generation of network desynchronization[1,4], thereby extending previous work that has demonstrated the role of both cholinergic receptors in cholinergic desynchronization[24]. Our finding (**Fig. 2c** and **Supplementary Fig. 10**) also agrees with parallel observations of state-dependent SOM activation[37,38] and state-dependent variation in cholinergic output in the cortex[39], where more awake states favor both greater ACh release and higher SOM activity. Our findings, however, do not rule out other alternative mechanisms that can underlie the generation of synchronization and desynchronization. In fact, rhythmic-bursting layer 5 pyramidal neurons[2], thalamocortical pathways[40], intracortical glutamatergic inputs[41] and direct/indirect neuromodulatory inputs[2], including serotonin pathways[42], can contribute to global changes in cortical state. Furthermore, slow oscillations originating in deeper cortical layers[43] can propagate[44] and interact with distinct cholinergic-activated cortical circuits across layers to lead to layer-specific patterns of cortical activation.

By performing local optogenetic stimulation of ChAT-ChR2 axons in the superficial layers of V1, we were able to focus on how cortical microcircuits can contribute to cholinergic desynchronization at a local scale. We identified the SOM neuron–driven microcircuit as

being important for local cholinergic desynchronization; however, it is possible that other factors, including intrinsic properties of PYR neurons[45], may also contribute to the phenomenon at a global level.

The co-existence of neuronal decorrelation and LFP desynchronization during ACh-induced SOM activation supports co-variation of temporal population activity with cortical states[4] and function[46]. Global cortical fluctuations have been proposed to induce neuronal correlations[4]. During cholinergic modulation, these global fluctuations are suppressed, as reflected by a decrease in large-amplitude, low-frequency activity (**Fig. 1d**)[2] thereby leading to neuronal decorrelation[4]. Small-amplitude, high-frequency activity then dominates[2] in the decorrelated states. Previous findings have, however, revealed the existence of highly correlated neuronal pairs in decorrelated states[10]. Future work will be necessary to characterize possible cell assemblies in the ACh-induced decorrelated states.

Our data agree with previous work that has demonstrated an increase in correlation when circuit inhibition is reduced[12] and suggest that SOM-activated pathways can provide a source of inhibition to induce decorrelation in the local circuit. Thus, a central question arising from this work is how the cholinergic-activated, SOM neuron–driven neural circuit can mediate temporal changes in neural activity. It is possible that this phenomenon may share common mechanisms with those mediating surround responses of V1 neurons. ACh enhances surround suppression[47], which is mediated by SOM neurons[37]. Activation of the surround reduces spike activity, but can induce decorrelation[48] and increase high-frequency components of the LFP[49]. Our results bridge these observations with evidence that SOM neurons can also mediate temporal alteration of cortical activity via cholinergic modulation, thereby suggesting that ACh-evoked, top-down cholinergic modulation in the temporal domain and visual stimulus–evoked, bottom-up modulation in the spatial domain may share the same circuit mechanisms involving SOM neurons.

Our findings also help to reconcile seemingly contradictory effects of cholinergic modulation and nucleus basalis stimulation on V1 neurons[7]. Cortical cholinergic activation has been linked to both GABA-mediated suppression[3,50] and facilitation of visual responses of V1 neurons[7,47,50]. These findings can, in principle, be explained by our finding that direct cholinergic activation of SOM neurons can drive both direct inhibition and possibly indirect disinhibition[19] on PYR neurons to vary their firing rate according to the relative strengths of the two pathways. Our results also extend the conclusions of earlier slice studies[15,16] that demonstrated excitation of non-FS inhibitory neurons and induction of an inhibitory barrage in FS and pyramidal neurons by ACh.

It is worth mentioning that mAChR-mediated facilitatory responses have also been observed in PYR neurons at a slower time scale[25,32–34] than that considered in our work. These responses have been shown to be mediated by both direct actions of ACh on PYR neurons and indirect actions via cortical astrocytes to drive ACh-induced plasticity[25,33,34] (**Supplementary Fig. 8b**,**e**,**h**). Together with our data showing SOM neurons as a dominant driver of both decorrelation and desynchronization in cortical networks, these findings suggest that the diffuse cholinergic innervation of cortex is transformed by distinct ACh-responsive cell types and their specialized microcircuits, acting across distinct time scales, to enable highly specific brain functions.

METHODS

Methods and any associated references are available in the online version of the paper.

ACKNOWLEDGMENTS

We thank G. Feng and H. Robertson (Massachusetts Institute of Technology) for providing ChAT-ChR2 mice, E. Boyden and A. Yang (Massachusetts Institute of Technology) for providing Arch virus, C. Le for technical assistance with viral injections and immunohistochemistry, S. El Boustani, R. Huda and M. Goard of the Sur laboratory for careful reading of manuscript and critical technical advice, T. Emery for technical assistance with the optogenetics laser setup, and J. Sharma for technical assistance. We especially thank B. Sabatini, A. Granger, W. Xu and Z. Fu for providing critical technical advice. This work was supported by an A*STAR (Singapore) Fellowship (N.C.), and grants from the US National Institutes of Health (R01EY007023, R01EY018648, U01NS090473), the National Science Foundation (EF1451125) and the Simons Foundation (M.S.).

AUTHOR CONTRIBUTIONS

N.C. and H.S. designed, conducted and analyzed the *ex vivo* experiments. H.S. and N.C. designed, conducted and analyzed the *in vivo* experiments. N.C., H.S. and M.S. wrote the manuscript. M.S. supervised the project.

COMPETING FINANCIAL INTERESTS

The authors declare no competing financial interests.

1. Kitt, C.A., Höhmann, C., Coyle, J.T. & Price, D.L. Cholinergic innervation of mouse forebrain structures. *J. Comp. Neurol.* **341**, 117 (1994).
2. Metherate, R., Cox, C. & Ashe, J. Cellular bases of neocortical activation: modulation of neural oscillations by the nucleus basalis and endogenous acetylcholine. *J. Neurosci.* **12**, 4701–4711 (1992).
3. Goard, M. & Dan, Y. Basal forebrain activation enhances cortical coding of natural scenes. *Nat. Neurosci.* **12**, 1444 (2009).
4. Harris, K.D. & Thiele, A. Cortical state and attention. *Nat. Rev. Neurosci.* **12**, 509–523 (2011).
5. Herrero, J.L. *et al.* Acetylcholine contributes through muscarinic receptors to attentional modulation in V1. *Nature* **454**, 1110 (2008).
6. Cohen, M.R. & Maunsell, J.H.R. Attention improves performance primarily by reducing interneuronal correlations. *Nat. Neurosci.* **12**, 1594–1600 (2009).
7. Thiele, A. Optimizing brain processing. *Nat. Neurosci.* **12**, 1359–1360 (2009).
8. Li, C.Y., Poo, M.M. & Dan, Y. Burst spiking of a single cortical neuron modifies global brain state. *Science* **324**, 643–646 (2009).
9. Gentet, L.J., Avermann, M., Matyas, F., Staiger, J.F. & Petersen, C.C.H. Membrane potential dynamics of GABAergic neurons in the barrel cortex of behaving mice. *Neuron* **65**, 422–435 (2010).
10. Renart, A. *et al.* The asynchronous state in cortical circuits. *Science* **327**, 587–590 (2010).
11. King, P.D., Zylberberg, J. & DeWeese, M.R. Inhibitory interneurons decorrelate excitatory cells to drive sparse code formation in a spiking model of V1. *J. Neurosci.* **33**, 5475–5485 (2013).
12. Sippy, T. & Yuste, R. Decorrelating action of inhibition in neocortical networks. *J. Neurosci.* **33**, 9813–9830 (2013).
13. Klausberger, T. *et al.* Brain state– and cell type–specific firing of hippocampal interneurons *in vivo*. *Nature* **421**, 844–848 (2003).
14. Cardin, J.A. *et al.* Driving fast-spiking cells induces gamma rhythm and controls sensory responses. *Nature* **459**, 663–667 (2009).
15. Arroyo, S., Bennett, C., Aziz, D., Brown, S.P. & Hestrin, S. Prolonged disynaptic inhibition in the cortex mediated by slow, non-α7 nicotinic excitation of a specific subset of cortical interneurons. *J. Neurosci.* **32**, 3859–3864 (2012).
16. Xiang, Z., Huguenard, J.R. & Prince, D.A. Cholinergic switching within neocortical inhibitory networks. *Science* **281**, 985–988 (1998).
17. Kawaguchi, Y. Selective cholinergic modulation of cortical GABAergic cell subtypes. *J. Neurophysiol.* **78**, 1743–1747 (1997).
18. Fanselow, E.E., Richardson, K.A. & Connors, B.W. Selective, state-dependent activation of somatostatin-expressing inhibitory interneurons in mouse neocortex. *J. Neurophysiol.* **100**, 2640–2652 (2008).
19. Xu, H., Jeong, H.-Y., Tremblay, R. & Rudy, B. Neocortical somatostatin-expressing GABAergic interneurons disinhibit the thalamorecipient layer 4. *Neuron* **77**, 155–167 (2013).
20. Alitto, H.J. & Dan, Y. Cell type–specific modulation of neocortical activity by basal forebrain input. *Front. Syst. Neurosci.* **6**, 79 (2012).
21. Fu, Y. *et al.* A cortical circuit for gain control by behavioral state. *Cell* **156**, 1139–1152 (2014).
22. Arroyo, S., Bennett, C. & Hestrin, S. Nicotinic modulation of cortical circuits. *Front. Neural Circuits* **8**, 30 (2014).
23. Letzkus, J.J. *et al.* A disinhibitory microcircuit for associative fear learning in the auditory cortex. *Nature* **480**, 331–335 (2011).
24. Kalmbach, A. & Waters, J. Modulation of high-and low-frequency components of the cortical local field potential via nicotinic and muscarinic acetylcholine receptors in anesthetized mice. *J. Neurophysiol.* **111**, 258–272 (2014).
25. Chen, N. *et al.* Nucleus basalis–enabled stimulus-specific plasticity in the visual cortex is mediated by astrocytes. *Proc. Natl. Acad. Sci. USA* **109**, 2832–2841 (2012).

26. Pfeffer, C.K., Xue, M., He, M., Huang, Z.J. & Scanziani, M. Inhibition of inhibition in visual cortex: the logic of connections between molecularly distinct interneurons. *Nat. Neurosci.* **16**, 1068–1076 (2013).
27. Jiang, X., Wang, G., Lee, A.J., Stornetta, R.L. & Zhu, J.J. The organization of two new cortical interneuronal circuits. *Nat. Neurosci.* **16**, 210–218 (2013).
28. Pi, H.-J. *et al.* Cortical interneurons that specialize in disinhibitory control. *Nature* **503**, 521–524 (2013).
29. Kruglikov, I. & Rudy, B. Perisomatic GABA release and thalamocortical integration onto neocortical excitatory cells are regulated by neuromodulators. *Neuron* **58**, 911–924 (2008).
30. Fino, E. & Yuste, R. Dense inhibitory connectivity in neocortex. *Neuron* **69**, 1188–1203 (2011).
31. Aramakis, V.B., Bandrowski, A.E. & Ashe, J.H. Muscarinic reduction of GABAergic synaptic potentials results in disinhibition of the AMPA/kainate-mediated EPSP in auditory cortex. *Brain Res.* **758**, 107–117 (1997).
32. McCormick, D.A. & Prince, D.A. Mechanisms of action of acetylcholine in the guinea-pig cerebral cortex *in vitro*. *J. Physiol. (Lond.)* **375**, 169–194 (1986).
33. Giessel, A.J. & Sabatini, B.L. M1 Muscarinic receptors boost synaptic potentials and calcium influx in dendritic spines by inhibiting postsynaptic sk channels. *Neuron* **68**, 936 (2010).
34. Buchanan, K.A., Petrovic, M.M., Chamberlain, S.E.L., Marrion, N.V. & Mellor, J.R. Facilitation of long-term potentiation by muscarinic m1 receptors is mediated by inhibition of sk channels. *Neuron* **68**, 948 (2010).
35. de La Rocha, J., Doiron, B., Shea-Brown, E., Josić, K. & Reyes, A. Correlation between neural spike trains increases with firing rate. *Nature* **448**, 802–806 (2007).
36. Rudy, B., Fishell, G., Lee, S. & Hjerling-Leffler, J. Three groups of interneurons account for nearly 100% of neocortical GABAergic neurons. *Dev. Neurobiol.* **71**, 45–61 (2011).
37. Adesnik, H., Bruns, W., Taniguchi, H., Huang, Z.J. & Scanziani, M. A neural circuit for spatial summation in visual cortex. *Nature* **490**, 226–231 (2012).
38. Gentet, L.J. *et al.* Unique functional properties of somatostatin-expressing GABAergic neurons in mouse barrel cortex. *Nat. Neurosci.* **15**, 607–612 (2012).
39. Marrosu, F. *et al.* Microdialysis measurement of cortical and hippocampal acetylcholine release during sleep-wake cycle in freely moving cats. *Brain Res.* **671**, 329–332 (1995).
40. Poulet, J.F.A., Fernandez, L.M.J., Crochet, S. & Petersen, C.C.H. Thalamic control of cortical states. *Nat. Neurosci.* **15**, 370–372 (2012).
41. Harris, K.D. Top-down control of cortical state. *Neuron* **79**, 408–410 (2013).
42. Vanderwolf, C.H. & Stewart, D. Thalamic control of neocortical activation: a critical re-evaluation. *Brain Res. Bull.* **20**, 529–538 (1988).
43. Compte, A., Sanchez-Vives, M.V., McCormick, D.A. & Wang, X.-J. Cellular and network mechanisms of slow oscillatory activity (< 1 Hz) and wave propagations in a cortical network model. *J. Neurophysiol.* **89**, 2707–2725 (2003).
44. Sakata, S. & Harris, K.D. Laminar structure of spontaneous and sensory-evoked population activity in auditory cortex. *Neuron* **64**, 404–418 (2009).
45. McCormick, D.A. Neurotransmitter actions in the thalamus and cerebral cortex and their role in neuromodulation of thalamocortical activity. *Prog. Neurobiol.* **39**, 337 (1992).
46. Fries, P., Reynolds, J.H., Rorie, A.E. & Desimone, R. Modulation of oscillatory neuronal synchronization by selective visual attention. *Science* **291**, 1560–1563 (2001).
47. Roberts, M.J. *et al.* Acetylcholine dynamically controls spatial integration in marmoset primary visual cortex. *J. Neurophysiol.* **93**, 2062–2072 (2005).
48. Vinje, W.E. & Gallant, J.L. Sparse coding and decorrelation in primary visual cortex during natural vision. *Science* **287**, 1273–1276 (2000).
49. Gieselmann, M.A. & Thiele, A. Comparison of spatial integration and surround suppression characteristics in spiking activity and the local field potential in macaque V1. *Eur. J. Neurosci.* **28**, 447–459 (2008).
50. Müller, C.M. & Singer, W. Acetylcholine-induced inhibition in the cat visual cortex is mediated by a GABAergic mechanism. *Brain Res.* **487**, 335–342 (1989).

ONLINE METHODS

Mice. *In vivo* experiments involving local field potential, single unit and cell-attached recordings were performed on adult mice between 2–6 months old. Slice experiments involving whole-cell patch clamp recordings were performed on P13–28 mice. Mice of both genders were used. These animals were housed under 12/12-h light/dark cycle and up to five animals per cage. The following mouse lines were used. **Figure 1**: ChAT-ChR2-EYFP line 6 (ChAT-ChR2)[51]. **Figures 2** and **3**: SOM-TD and VIP-TD mice were generated by crossing the CAG- tdTomato +/+ mice[52] (td, Jackson Labs) with SOM-Cre knockin driver mice (SOM-Cre+/+, Jackson Labs) and VIP-Cre knockin driver mice (VIP-Cre+/+, Jackson Labs); Arch-GFP was expressed in SOM neurons by injecting the AAV8-CAG-FLEX-Arch-GFP virus (Arch, E. Boyden, Massachusetts Institute of Technology and University of North Carolina Vector Core)[53] into SOM-Cre+/− mice; or into GAD-67-GFP-SOM-Cre mice generated by first crossing GAD-67-GFP with SOM-Cre+/+ mice; C57BL6 (WT). **Figure 4**: ChAT-ChR2; ChAT-ChR2-SOM-Cre and ChAT-ChR2-PV-Cre mice were generated by crossing ChAT-ChR2 +/− mice with SOM-Cre+/+ and PV-Cre knockin driver mice (PV +/+, Jackson Labs) respectively[54]. Viral injection of the rAAV9/LS2L-dsRed-Exp virus (University of North Carolina Vector Core) containing the *loxP-STOP-loxP-RFP* construct[55,56] was used to label SOM or PV neurons with RFP. **Figure 5**: Arch-GFP was expressed in SOM neurons by injecting the Arch virus into ChAT-ChR2-SOM-Cre-mice generated by crossing ChAT-ChR2 +/− with SOM-Cre +/+ mice. **Figure 6**: Arch-GFP was expressed in VIP neurons by injecting the Arch virus into ChAT-ChR2-VIP-Cre-mice generated by crossing ChAT-ChR2 +/− with VIP-Cre +/+ mice. **Figure 7**: ChR2 was expressed in SOM neurons by injecting the AAV1.EF1.dflox.hChR2(H134R)-mCherry.WPRE.hGH virus (Penn Vector Core) into SOM-Cre +/− mice. **Supplementary Figure 5**: SOM-TD; PV-TD mice were generated by crossing the td mice with PV-Cre+/+; GAD-67-GFP[57] or C57BL6 (WT). **Supplementary Figure 6**: RFP was expressed in SOM neurons by injecting the *AAV-LS$_2$L-RFP* virus into ChAT-ChR2-SOM-Cre-mice; SOM-TD. **Supplementary Figure 13**: Arch-GFP was expressed in VIP and 5HT3aR-expressing neurons by injecting the AAV-CAG-FLEX-Arch-GFP virus (Arch) into VIP-Cre+/− mice and 5HT3aR-Cre knockin driver mice (5HT3aR-Cre+/−, Gensat); All experiments were performed under protocols approved by the Animal Care and Use Committee at the Massachusetts Institute of Technology and conformed to US National Institutes of Health guidelines.

Viral injection. The procedure was similar to that described earlier[54,55]. Briefly, adult mice were anesthetized in isoflurane before the skull was thinned and the dura in primary visual cortex (V1) was punctured using a glass micropipette filled with virus. A volume of 0.25 µl of virus was injected at the depth of 250 µm. Experiments were performed at least 2 weeks post-injection.

***In vivo* surgery.** Mice were anesthetized with urethane (1.15 mg per g of body weight). Ophthalmic ointment was used to protect the animal's eyes during the surgery and replaced with silicon oil during imaging. Body temperature was maintained at 37.5 °C with a heating pad. A metal headplate was attached to the skull with cyanoacrylate glue and dental acrylic. A 2 × 2 mm craniotomy was made over V1 which was later covered with a thin layer of 2% agarose in ACSF (140 mM NaCl, 5 mM KCl, 2 mM $CaCl_2$, 1 mM $MgCl_2$, 0.01 mM EDTA, 10 mM HEPES, 10 mM glucose, pH 7.4).

***In vivo* cell-attached recording and data analysis.** Glass pipettes (1.5-µm tip size, 3–7 MΩ) filled with Alexa dye 488 (A488, Invitrogen) and held at positive pressure were visually-guided into V1 with a two-photon scanning microscope (Sutter Instruments) using ScanImage software (K. Svoboda, Janelia Farm)[58] and directed to 100–200 µm below the pial surface (layer 2/3) using a micromanipulator[55]. Cells were imaged using a 25×, 0.95-N.A. lens (Olympus Optical) at an excitation wavelength of 910 nm. The fluorescence was detected using photomultiplier tubes (R6357; Hamamatsu). The resistance of the pipette was monitored during the penetration by delivering −0.5 nA current pulses for 6.3 ms at 0.55 Hz with Clampex software (Axon Instruments, v8.1) and Axoclamp-2A amplifier (Axon Instruments). When a seal during the advancement of pipette was obtained (assessed by increase in pipette tip resistance) and well-isolated spikes were detected on Clampex during visual stimuli presentation, sustained negative pressure was applied (0.2–0.6 psi) to secure the seal[59]. To fill the recorded cells, current pulses (35 ms, 900–2,000 nA) were delivered at 15 Hz for 30–60 s. Recordings were performed at a sampling rate of 30 kHz and filtered between 300 Hz and 10 kHz. The pClamp data was analyzed with Clampfit software v 10.2 (MDS Analytical Technologies) for spike detection and the analyzed data was then imported in Matlab and further analyzed with custom-written scripts. In **Figure 4c**, firing rates were normalized by the mean firing rate across 8s of spontaneous responses before ChAT-ChR2 stimulation. In **Figures 4f**,**i**, firing rates were normalized by the mean visual responses before ChAT-ChR2 stimulation.

***In vivo* single-unit recording and data analysis.** Single-unit extracellular recordings[25] were made using tungsten microelectrodes (0.8 MΩ, FHC). The signal was amplified and recorded using the Plexon Neurotechnology Research Systems (4–8 channels, 40 kHz at 12-bit resolution, Plexon). The signal was thresholded using an online amplitude discriminator and played over an integrated stereo amplifier (Optimus). Offline analysis to sort waveforms for each unit was performed using commercial programs (Offline Sorter version 2.8.8, Plexon).

Post processing was performed with in-house code written in MATLAB. Units were selected by two criteria for further analysis: visual responsiveness (paired *t* test, $P < 0.05$) and firing rate (>0.1 Hz). To avoid artifacts due to the same unit being picked up by more than one electrode, we removed units which had high correlation with others (pair-wise between-units correlation coefficient >0.1, with 1 kHz bin). For correlation analysis across units, we first binned responses at 100 ms (10 Hz) (**Fig. 1f** and **Supplementary Fig. 1g**) before the mean Pearson correlation coefficient for each cell was calculated using all pairs of responses between the cell and other cells recorded simultaneously[3]. Population averaged correlation coefficients in **Figures 1g** and **5g** and **Supplementary Figures 1i** and **11f** were computed by first averaging the correlation coefficient across all cells recorded simultaneously before taking the mean of these averaged correlation coefficients for each experiment. The single Pearson correlation coefficients between all pairs of responses are also plotted in **Supplementary Figure 1h** and **12b**.

The discrimination analysis in **Supplementary Figure 12d** was computed as previously reported[3]. Responses were first binned in 100-ms segments. Discriminability was then calculated by comparing the similarity of single-trial responses to two templates comprising mean trial-averaged responses. Each discrimination was quantified by calculating the Euclidean distance between (a) single-trial responses in a given bin and the mean trial-averaged responses in the same bin, and between (b) the single-trial responses and the mean trial-averaged responses in a different bin. Discrimination was assigned correct when the distance (a) was smaller than distance (b). The discrimination performance of both control and light-stimulated experiments was normalized by the maximum performance of the control experiment for comparison. Data sets with more than 9 units were used for this analysis. Two-way ANOVA was used to assess effect of number of units included to calculate discrimination performance, and effect of light stimulation.

***In vivo* LFP recording and data analysis.** The LFP recordings were made using a glass pipette (2.5–3-µm tip size, 2–3 MΩ) to prevent optogenetic laser stimulation–induced artifacts[60]. The pipette, filled with A488 and Alexa dye 594 (A594), was visually guided into V1 with a microscope and directed 100–200 µm below the pial surface (layer 2/3) using a micromanipulator. A single channel on the Plexon Neurotechnology Research Systems was used to amplify and record the signal. The LFP signal before and during laser stimulation (1–3 s) was analyzed using in-house code written in MATLAB to construct the power spectrum.

Visual and optogenetic stimulation. Natural movies and random orientation gratings were displayed on a 19-inch LCD monitor situated 15 cm from the eyes. Experiments with natural stimuli consisted of 40–60 trials where each trial comprised a set each of control and optogenetic stimulation conditions. Each set comprised three 5-s natural movies (128 × 128 pixels) selected from the van Hateren natural movie database. Each movie was preceded by a control period consisting of 3 s of blank gray screen and 2 s of still image of the first movie frame to avoid onset effects. Multiple trials were performed with alternating absence and presence of ChAT-ChR2 stimulation synchronized to the start of each movie (see **Fig. 1e**). Arch stimulation preceded by 1 s and continued for the duration of the ChAT-ChR2 stimulation so as to ensure suppression of SOM neurons during this period.

Experiments with random orientation gratings consisted of 40–60 trials where each trial comprised three repeats of alternating 4 s of blank screen and

4 s of random orientation grating presentation. ChAT-ChR2 stimulation was synchronized to the start of the third repeat of grating presentation (**Fig. 1e**). Arch stimulation preceded by 1s and continued for the duration of the ChAT-ChR2 stimulation. Random orientation grating stimuli were generated with the Psychophysics toolbox[61] in Matlab. The stimuli consisted of square wave drifting gratings at 100% contrast in eight randomly permuted directions, each 45 degrees apart and lasting for 450 ms.

To perform optogenetic stimulation of ChR2 and Arch, we used diode-pumped solid state blue and green lasers with analog intensity control (MBL-III-473 (blue, 473 nm) and MBL-III-532 (green, 532 nm), OptoEngine, LLC). The stimulation parameters are as follows. Blue light: 1–5-s duration, 20 Hz, 10-ms pulse width, 1 mW mm^{-2} (used in **Fig. 7**), 10 mW mm^{-2} (low ChAT-ChR2 stimulation intensity, used in all figures except **Fig. 7** and **Supplementary Fig. 10**), 30–60 mW mm^{-2} (high ChAT-ChR2 stimulation intensity, used in **Supplementary Fig. 10**); green light: 5–15-s duration, continuous light, 0.1–1 mW mm^{-2}. Pulse patterns were driven via custom D/A optogenetics software written in Matlab. The onset of visual stimuli was synchronized to the initiation of cell-attached spike, single unit, LFP recordings and optogenetic stimulation via trigger pulses. Blue laser light was focused onto superficial layers of V1 using a 10× objective lens. The estimated area is approximately 0.8 mm^2.

Blue light stimulation of V1 in ChAT-ChR2 (ref. 62) mice leads to photoactivation of cholinergic axons from the basal forebrain and a small, localized set of intrinsic cholinergic interneurons. The functional consequences of the activation of the intrinsic cholinergic interneurons have, however, been shown to be limited[63,64].

Slice physiology. Coronal slices (300 μm) of visual cortex were cut in slicing buffer (<4 °C, perfused with carbogen comprising 95% O_2/5% CO_2, pH 7.33–7.38) with a vibratome (Leica VT 1200S) and incubated in artificial cerebral spinal fluid (ACSF) at 25 °C for at least 30 min before being transferred to a slice chamber for patch recordings. All experiments were performed in carbogen-perfused ACSF. The ACSF contained (in mM): NaCl, 130; $NaHCO_3$, 24; KCl, 3.5; NaH_2PO_4, 1.25; Glucose, 10; $CaCl_2$, 2.5; $MgCl_2$, 1.5. The slicing buffer was of similar composition as ACSF except (in mM): $CaCl_2$, 1; $MgCl_2$, 5. The low chloride intracellular pipette (internal) solution for patching neurons in current clamp mode contained (in mM): KCl, 20; potassium gluconate, 100; HEPES, 10; Mg-ATP: 4; Na-GTP: 0.3; Na-Phosphocreatine, 10, pH 7.4, 295 mOsm. EPSCs were recorded in voltage clamp mode (holding potential −70 mV) with the low-chloride internal solution. For recording IPSCs in voltage-clamp mode (holding potential −70 mV, in the presence of NBQX), a high-chloride internal solution was used (in mM): KCl, 120; HEPES, 10; Mg-ATP: 4; Na-GTP: 0.3; sodium phosphocreatine, 10, pH 7.4, 295 mOsm. Drugs: ACh (1 μM to 10 mM), atropine sulfate (atropine, 50 μM), mecamylamine hydrochloride (Meca, 10 μM), bicuculline methiodide (BCC, 20 μM) and tetrodotoxin (TTX, 1 μM) were purchased from Sigma; D-(−)-2-amino-5-phosphonopentanoic acid (D-AP5, 50 μM), 2,3-dioxo-6-nitro-1,2,3,4-tetrahydrobenzo[*f*]quinoxaline-7-sulfonamide disodium salt (NBQX, 10 μM), gabazine (10 μM) and CGP55845 hydrochloride (2 μM) were purchased from Tocris. Drugs were bath applied, except for ACh which was applied by pressure injection with a picospritzer.

Intracellular recording in slices. Glass pipettes (4 – 7 MΩ) were pulled with a Sutter P1000 puller (Sutter instruments). Layer 2/3 cells were visualized with an Olympus BX61WI microscope coupled with a 40× water immersion lens (Olympus), infrared-DIC optics and CCD camera (Qimaging).

In GAD-67-GFP-SOM-Cre-Arch slices used in **Figure 2i–k**, putative VIP neurons were identified by their expression of GFP, their RS characteristic and lack of hyperpolarizing response to green light stimulation. In GAD-67-GFP-SOM-Cre-Arch slices used in **Figure 3c–e**, FS neurons were identified by their expression of GFP and their FS characteristic. In SOM-Cre-Arch slices in **Figure 3f–h**, in GAD-67-GFP slices in **Supplementary Figure 5k–m**, in VIP-Cre-Arch slices in **Supplementary Figure 13c**,**d** and in 5HT3aR-Cre-Arch slices in **Supplementary Figure 13g**,**h**, regular-spiking (RS) putative excitatory neurons (PYR) were identified by the absence of GFP as well as their morphological and electrophysiological characteristics: pyramidal-shaped soma, apical dendrites radially projecting toward the pial and basal dendrites directed downwards and laterally[65] and adaptation of spike frequency when stimulated with a constant current[66]. A subset of experiments in **Supplementary Figure 5k–m** was performed in C57BL/6 slices where PYR neurons were identified by their distinct morphological and electrophysiological characteristics as described above.

Recordings were performed with a multiclamp 700B amplifier and digidata 1440A data acquisition system, with pClamp software in both the current- and voltage-clamp modes. Optogenetic stimulation of Arch was performed using output from a Lumen 200 fluorescence lamp (5% light output, Prior Scientific) through a green filter.

Slice physiology analysis. Analysis was performed with the Clampfit 10.2.0.12 software. In **Figures 2c**,**e**,**h**,**k**,**n** and **3b**,**e**,**h**, and **Supplementary Figures 3**, **4c**, **6b**, **7**, **8c**,**f**,**i** and **13b**,**d**,**f**,**h**,**j**, the ACh induced changes in response was defined as (Ach response) $_{\text{after drug}}$ − (Ach response) $_{\text{before drug}}$ where (Ach response) was computed over 10 s. **Supplementary Figure 6c–e** was analyzed using the Mini Analysis Program (Synaptosoft, v 6.0.7): The latency was defined as the time to reach peak amplitude and computed by finding the first data point to the left of the peak that showed 0.5% of the peak amplitude before subtracting the time at this point from the time at the peak. The peak amplitude was calculated by taking the amplitude at the local maximum minus the average baseline. The charge was computed as the area under the curve by taking an integral of amplitude from the first data point to the left of the peak that showed 0.5% of the peak amplitude to the first data point to the right of the peak that showed 0.37 of the peak amplitude.

Immunohistochemistry. SOM-TD mice (P34; **Supplementary Fig. 6f**) were anesthetized with 4% isoflurane and perfused transcardially with saline followed by chilled 4% paraformaldehyde in 0.1 M phosphate-buffered saline (PBS). The brains were then postfixed in 4% paraformaldehyde in 0.1 M PBS (<4 °C) overnight. The fixed brains were sectioned into 50 μm visual cortical slices with a vibratome and then blocked in 10% normal goat serum with 1% triton in PBS (1 h, 25 °C) before being stained with rabbit anti-M1 and anti-M2 (1:200, Millipore, AB5164, AB5166) or rabbit anti-nAChR alpha4 and rabbit anti-nAChR beta2 or rabbit anti-nAChR alpha7 (1:200, Abcam, ab41172, ab55980, ab23832)[67] overnight (<4 °C). This was followed by a 3-h incubation in Alexa Fluor 488 goat anti-rabbit (1:200, Invitrogen, A11034) before being mounted on a glass slide with the Vectashield Hardset mounting media (Vector Labs). The slides were imaged using a confocal microscope (Zeiss LSM 5 Pascal Exciter) and the images were analyzed for co-localization of tdTomato-positive SOM neurons and the respective cholinergic receptors stains.

Statistics and general method. Detailed sampling statistics for all figures are provided in **Supplementary Tables 1** and **2**. The normality test was performed to check if samples can be described by a Gaussian distribution before the standard *t* test was used to compare responses across populations of neurons and across animals. Two-tailed, paired *t* test was used for comparisons unless indicated. In a small subset of experiments that did not pass the normality test, non-parametric statistics were used. Error bars indicate s.e.m. unless indicated. Blind experiments were not performed in the study but the same criteria were applied to all allocated groups for comparisons. No randomization was performed for the study. No statistical methods were used to predetermine sample sizes, but our sample sizes are similar to those reported in previous publications[21,37].

A **Supplementary Methods Checklist** is available.

51. Zhao, S. *et al.* Cell type-specific channelrhodopsin-2 transgenic mice for optogenetic dissection of neural circuitry function. *Nat. Methods* **8**, 745–752 (2011).
52. Madisen, L. *et al.* A robust and high-throughput Cre reporting and characterization system for the whole mouse brain. *Nat. Neurosci.* **13**, 133–140 (2010).
53. Chow, B.Y. *et al.* High-performance genetically targetable optical neural silencing by light-driven proton pumps. *Nature* **463**, 98–102 (2010).
54. Wilson, N.R., Runyan, C.A., Wang, F.L. & Sur, M. Division and subtraction by distinct cortical inhibitory networks *in vivo*. *Nature* **488**, 343–348 (2012).
55. Runyan, C.A. *et al.* Response features of parvalbumin-expressing interneurons suggest precise roles for subtypes of inhibition in visual cortex. *Neuron* **67**, 847–857 (2010).
56. Kuhlman, S.J. & Huang, Z.J. High-resolution labeling and functional manipulation of specific neuron types in mouse brain by Cre-activated viral gene expression. *PLoS One* **3**, e2005 (2008).
57. Tamamaki, N. *et al.* Green fluorescent protein expression and colocalization with calretinin, parvalbumin, and somatostatin in the GAD67-GFP knock-in mouse. *J. Comp. Neurol.* **467**, 60–79 (2003).

doi:10.1038/nn.4002

58. Pologruto, T.A., Sabatini, B.L. & Svoboda, K. ScanImage: flexible software for operating laser scanning microscopes. *Biomed. Eng. Online* **2**, 13 (2003).
59. Joshi, S. & Hawken, M.J. Loose-patch-juxtacellular recording *in vivo*: a method for functional characterization and labeling of neurons in macaque V1. *J. Neurosci. Methods* **156**, 37–49 (2006).
60. Cardin, J.A. *et al.* Targeted optogenetic stimulation and recording of neurons *in vivo* using cell type–specific expression of Channelrhodopsin-2. *Nat. Protoc.* **5**, 247–254 (2010).
61. Brainard, D.H. The Psychophysics Toolbox. *Spat. Vis.* **10**, 433 (1997).
62. Kalmbach, A., Hedrick, T. & Waters, J. Selective optogenetic stimulation of cholinergic axons in neocortex. *J. Neurophysiol.* **107**, 2008–2019 (2012).
63. von Engelhardt, J., Eliava, M., Meyer, A.H., Rozov, A. & Monyer, H. Functional characterization of intrinsic cholinergic interneurons in the cortex. *J. Neurosci.* **27**, 5633–5642 (2007).
64. Tricoire, L. & Cea-Del Rio, C.A. Illuminating cholinergic microcircuits in the neocortex. *J. Neurosci.* **27**, 12119–12120 (2007).
65. DeFelipe, J. & Fariñas, I. The pyramidal neuron of the cerebral cortex: morphological and chemical characteristics of the synaptic inputs. *Prog. Neurobiol.* **39**, 563–607 (1992).
66. Connors, B.W. & Gutnick, M.J. Intrinsic firing patterns of diverse neocortical neurons. *Trends Neurosci.* **13**, 99–104 (1990).
67. Prestori, F. *et al.* Gating of long-term potentiation by nicotinic acetylcholine receptors at the cerebellum input stage. *PLoS ONE* **8**, e64828 (2013).